Sensitivity Analysis for DSMC Simulations of High-Temperature Air Chemistry

James S. Strand[1] and David B. Goldstein[2]
The University of Texas at Austin, Austin, TX, 78712

This research centers on laying the groundwork for the application of Bayesian statistical methods for the calibration of parameters relevant to modeling a hypersonic shock layer with the Direct Simulation Monte Carlo (DSMC) method. The DSMC method used in this work employs the algorithm of Bird (1994), with modifications to allow integration with sensitivity analysis and Markov Chain Monte Carlo (MCMC) driver codes. The DSMC code was written and optimized with shock tube simulations in mind. Sensitivity analyses have been performed to determine which parameters most affect the simulation results for a 0-D relaxation which is similar in many respects to the relaxation behind a steady 1-D hypersonic shock. Analyses were performed for a pure nitrogen case and for a 5-species air case. The parameters which are most sensitive have been identified for future calibration with MCMC.

Introduction

It appears that little prior research work has been done which integrates Direct Simulation Monte Carlo (DSMC) with Bayesian statistical methods. If used properly, Bayesian methods could prove useful in improving DSMC.

The current work focuses on sensitivity analysis and on laying the groundwork for future parameter calibration. The DSMC method includes many parameters related to gas dynamics at the molecular level. Examples include elastic collision cross-sections, vibrational and rotational excitation probabilities, reaction cross-sections, etc. In many cases, the precise values of these parameters are not known. Parameter values often cannot be directly measured. Instead they must be inferred from experimental results, and by necessity parameters must often be used in regimes far from where their values were determined. More precise values for some of these important parameters could lead to better simulation of the physics, and thus to better predictive capability for DSMC.

In the future Bayesian methods could also be employed to evaluate the plausibility of various models within the context of DSMC simulations. For example, comparisons could be made between the total collision energy (TCE) model for reaction cross-sections which was described by Bird (1994) and used by Ozawa (2008), and the vibrationally favored dissociation model, also described by Bird (1994). Future model development could also be guided by information gleaned from application of Bayesian statistical analysis to existing models. Our current work, however, focuses on using Bayesian methods to provide improved calibrations for models which are already in common use.

Obtaining these calibrated parameters is the long-term goal of our work. In approaching that goal, the first step is a sensitivity analysis to determine which parameters most affect the simulation results in a case which is similar to a hypersonic shock. In this work, we have performed a rigorous sensitivity analysis in order to select appropriate parameters for calibration. This will set the stage for eventual calibrations with experimental data from the NASA EAST shock tube (see Grinstead et al., 2008) in future work.

Numerical Methods

DSMC

The DSMC code used in this work is based on the method described by Bird (1994). In order to facilitate integration with a sensitivity analysis driver code, and in the future with a Markov Chain Monte Carlo (MCMC) driver, the entire DSMC code is written as a subroutine.

The DSMC code is capable of handling multiple species, each with its own molecular properties. Both vibrational and rotational internal energies are included. The code also handles 5-species air chemistry, including dissociation, recombination, and exchange reactions (only dissociation and exchange reactions are modeled in the current work, however).

[1] Graduate Researcher, Aerospace Engineering Dept., 1 University Station, C0600, Student.
[2] Professor, Aerospace Engineering Dept., 1 University Station, C0600, Senior Member.

Elastic collisions in the code are performed using the VHS collision model, described in Bird (1994). VHS parameters for the 5 species used in this work are shown in Table 1. In general, VHS parameters for cross-species collisions are obtained by a simple averaging of the parameters for the two species participating in the collision, but the code is capable of employing specific (non-averaged) values for the cross-collision VHS parameters. In the sensitivity analysis presented later for the pure nitrogen case, the VHS parameters for N_2-N collisions are treated separately from the parameters for N_2-N_2 and N-N collisions. As shown in Table 3, we check sensitivity to the VHS parameters (d_{ref} and ω) which apply to N_2-N_2 collisions, the parameters which apply to N-N collisions, and also the parameters which apply to N_2-N collisions. That is, during the pure nitrogen sensitivity analysis, we do not assume that the VHS parameters for N_2-N collisions are simply the average of the parameters for N_2-N_2 and N-N collisions. In the 5-species case, however, where we do not check sensitivity for the VHS parameters, this assumption is made. In that case, the VHS parameters for all cross-species collisions are the arithmetic average of the VHS parameters for the two species involved in the collision.

Table 1: VHS parameters for 5-species air.

Species	ω	d_{ref} ($\times 10^{-10}$ m)	T_{ref} (K)
N_2	0.65	3.11	1000
N	0.68	3.58	1000
O_2	0.65	2.96	1000
O	0.68	3.37	1000
NO	0.65	3.41	1000

Bird (1994) lays out the details of the Larsen-Borgnakke model (Borgnakke and Larson, 1975) for application to the modeling of particles with internal degrees of freedom within the DSMC framework. This model is phenomenological in nature. The key aspect of the model is that some fraction of collisions are regarded as inelastic, and in these collisions energy may be redistributed between the translational and internal modes. This redistribution is carried out based on selections of post-collision internal energies from the equilibrium distributions appropriate for the given mode at the collision energy. After the internal energies have been assigned, the remaining energy is assigned to the relative translational kinetic energy of the colliding particles. It is important to emphasize that, for a given inelastic collision, the post-collision energies are chosen from a distribution based on the energy of *that particular collision*, rather than a distribution based on the overall cell properties. This allows significant non-equilibrium to be present between the internal and translational modes at a given point in the flowfield.

The treatment of rotational and vibrational energies in our DSMC code follows the implementation of Bird (1994), described above. Rotation is assumed to be fully excited. Each particle has its own value of rotational energy, and this variable is continuously distributed (rotation is not considered quantized due to the close spacing of rotational levels). Particles have either zero rotational degrees of freedom (monatomic species) or two degrees of freedom (diatomic species). The code does not currently model species with three rotational degrees of freedom, because there are no species relevant to the current work which have more than two atoms, and all diatomic species have two rotational degrees of freedom, regardless of whether they are homonuclear or heteronuclear.

Some fraction of collisions are considered inelastic, and in some of these collisions rotational energy is redistributed between the translational and rotational modes. The redistribution is based on the Larsen-Borgnakke model. The parameter relevant to rotational excitation is Z_R, the rotational collision number. In both our code and that of Bird, Z_R is defined as $1/\lambda_R$, where λ_R is the probability of a given molecule's rotational energy undergoing redistribution with the translational mode during any given collision. In our code, Z_R can be defined as constant for all species, as collision partner dependent (but independent of collision temperature), as collision temperature dependent (but independent of collision partner), or as dependent on both collision partner and collision temperature.

Vibration, on the other hand, is not assumed to be fully excited, and vibrational levels are quantized. Each particle has its own vibrational level, which is associated with a certain vibrational energy based on the simple harmonic oscillator model. As with rotation, in some fraction of collisions energy is redistributed between the translational and vibrational modes. During an inelastic (but non-reactive) collision in which vibrational energy is redistributed, the post-collision vibrational level of a particle is not allowed to be chosen such that its vibrational energy would be greater than the dissociation energy for its species. This is done because dissociation is accounted for separately with dissociation cross-sections obtained via the TCE model, which will be discussed shortly. These dissociation cross-sections are calculated with the intent of matching the Arrhenius rates for the dissociation reactions. Thus, allowing additional dissociation events during the Larsen-Borgnakke redistribution for inelastic

(but non-reacting) collisions would be "double-dipping", and could lead to significant overestimation of the dissociation rate. Like with rotation, Z_V, the vibrational collision number, may be treated as a constant, or it can be collision partner dependent, collision temperature dependent, or both. In the work described here, both Z_R and Z_V will be treated as constants for all species and collision temperatures.

As mentioned above, chemistry is handled by means of the TCE model. This model treats the ratio of the cross-section for a given reaction to the total collision cross-section as a function of the total energy (translational and internal) of the two colliding particles. Bird (1994) lays out the process for determining the reaction cross-section as a function of the collision energy, and for determining the parameters of this function based on the parameters of an Arrhenius-type rate equation, of the form

$$K_f(T) = AT^{\eta} e^{E_A/k_B T}. \quad (1)$$

Arrhenius rates for the reactions important for high-temperature air chemistry have been tabulated, for example, by Ozawa et al. (2008), and these tabulated rate constants are used in this work to provide σ_R as a function of collision energy for all the required reactions. When sensitivity analysis and later MCMC calibrations are performed, the relevant parameters are the pre-exponential constants in the Arrhenius-type rate equations for the various reactions. We do not include the activation energy (E_A) or the temperature exponent (η) in the sensitivity analysis. In the case of E_A, this is because E_A is considered reasonably well known for diatomic species, at least in comparison to the uncertainties in the other Arrhenius rate parameters. In the case of η, this is because the effects of A and η on the reaction rates are very strongly coupled. If they were included in the sensitivity analysis, it would be necessary to more thoroughly examine coupling between parameters. This may be done in the future, but has not been done here. Table 2 contains the full list of reactions used in this work, along with relevant parameters for each reaction. The rates in Table 2 were tabulated from various sources by Ozawa et al. (2008). Many of the rates tabulated by Ozawa are for generic reaction types, such as O_2 dissociation, and are listed in their paper with equations like $M + O_2 \rightarrow M + O + O$. The reactions are all listed separately in Table 2 because we will check sensitivity to the reactions separately. Even if the nominal values of the Arrhenius parameters are the same for several similar reactions, we will check sensitivity to those reactions separately. The parameter α shown in Table 2 is used later in the sensitivity analysis, and is defined by the relationship $10^{\alpha} = A$.

Table 2: Reactions for 5-species air. Arrhenius rate data compiled by Ozawa et al. (2008).

Reaction #	Reaction Equation	A	α	η	E_A	$q_{reaction}$
1	$N_2 + N_2 \rightarrow N_2 + N + N$	1.16E-08	-7.93554	-1.6	1.56E-18	-1.56E-18
2	$N + N_2 \rightarrow N + N + N$	4.98E-08	-7.30277	-1.6	1.56E-18	-1.56E-18
3	$O_2 + N_2 \rightarrow O_2 + N + N$	4.98E-08	-7.30277	-1.6	1.56E-18	-1.56E-18
4	$O + N_2 \rightarrow O + N + N$	4.98E-08	-7.30277	-1.6	1.56E-18	-1.56E-18
5	$NO + N_2 \rightarrow NO + N + N$	4.98E-08	-7.30277	-1.6	1.56E-18	-1.56E-18
6	$N_2 + O_2 \rightarrow N_2 + O + O$	3.32E-09	-8.47886	-1.5	8.21E-19	-8.21E-19
7	$N + O_2 \rightarrow N + O + O$	3.32E-09	-8.47886	-1.5	8.21E-19	-8.21E-19
8	$O_2 + O_2 \rightarrow O_2 + O + O$	3.32E-09	-8.47886	-1.5	8.21E-19	-8.21E-19
9	$O + O_2 \rightarrow O + O + O$	3.32E-09	-8.47886	-1.5	8.21E-19	-8.21E-19
10	$NO + O_2 \rightarrow NO + O + O$	3.32E-09	-8.47886	-1.5	8.21E-19	-8.21E-19
11	$N_2 + NO \rightarrow N_2 + N + O$	8.30E-15	-14.0809	0	1.04E-18	-1.04E-18
12	$N + NO \rightarrow N + N + O$	8.30E-15	-14.0809	0	1.04E-18	-1.04E-18
13	$O_2 + NO \rightarrow O_2 + N + O$	8.30E-15	-14.0809	0	1.04E-18	-1.04E-18
14	$O + NO \rightarrow O + N + O$	8.30E-15	-14.0809	0	1.04E-18	-1.04E-18
15	$NO + NO \rightarrow NO + N + O$	8.30E-15	-14.0809	0	1.04E-18	-1.04E-18
16	$N_2 + O \rightarrow NO + N$	9.45E-18	-17.0246	0.42	5.93E-19	-5.21E-19
17	$O_2 + N \rightarrow NO + O$	4.13E-21	-20.384	1.18	5.53E-20	2.21E-19
18	$NO + N \rightarrow N_2 + O$	2.02E-17	-16.6946	0.1	0	5.21E-19
19	$NO + O \rightarrow O_2 + N$	1.40E-17	-16.8539	0	2.65E-19	-2.21E-19

A key assumption employed in the derivation of the equations for the TCE method (Bird, 1994) is that the reaction cross-section is much smaller than the elastic collision cross-section ($\sigma_R << \sigma_{VHS}$), or put another way, that $\sigma_{VHS} \approx \sigma_{Total}$. This assumption is not always completely accurate, especially at high temperatures. In order to test this assumption and examine how well the DSMC code reproduces the Arrhenius rates, we ran a series of single step runs at various temperatures. For each such run, a 0-D box is initialized with equal number fractions of N_2, N, O_2, O, and NO, and a total number density of 1.0×10^{23} #/m^3. The ratio of real to simulated particles is chosen so that there are ~10,000,000 simulated particles in the box. The code is then run for a single time step, and the number of each type of reaction is tabulated. These tabulated values are then ensemble averaged over a total of 400 single-step runs (each with a different random number seed). The time step chosen is short enough that the vast majority of particles do not undergo collisions or reactions; therefore the reaction counts can be converted to instantaneous rates at the initial temperature. The Arrhenius rates are expressed as functions of a single temperature, and they are not very meaningful when local thermal equilibrium does not exist. Therefore, in these test cases, all species are initialized with a given overall temperature. For the monatomic species, this is simply the translational temperature, but for the diatomic species, the distribution of internal states is initialized to an equilibrium at the given temperature (i.e. $T_{rot} = T_{vib} = T_{trans} = T_{ov}$). The TCE method does not assume require equilibrium, thermal equilibrium is only necessary in order for comparison with Arrhenius reaction rates.

The above process is performed at a total of 768 temperatures between 1000 K and 25000 K, and the results are compared with the predicted Arrhenius rates in Figures 1, 2, and 3. Agreement is very good for the nitrogen dissociation and oxygen dissociation reactions at all temperatures. There is more discrepancy between the DSMC and Arrhenius rates for the NO dissociation and the NO exchange reactions, and the discrepancy worsens at higher temperatures. This is due to the fact that, based on the Arrhenius rates tabulated by Ozawa (2008), these reactions have the highest rates of those examined, and at higher temperatures the assumption that $\sigma_R << \sigma_{VHS}$ becomes less and less accurate. In fact, for the reaction NO + NO → NO + N + O at 25000 K, σ_R is slightly greater than σ_{VHS}. Nonetheless, even for that reaction, the maximum difference between DSMC and Arrhenius rates is ~30%, and the difference is much less than that for most of the reactions. Given the very large uncertainties in the rates themselves, this level of discrepancy between Arrhenius and DSMC reactions is considered acceptable.

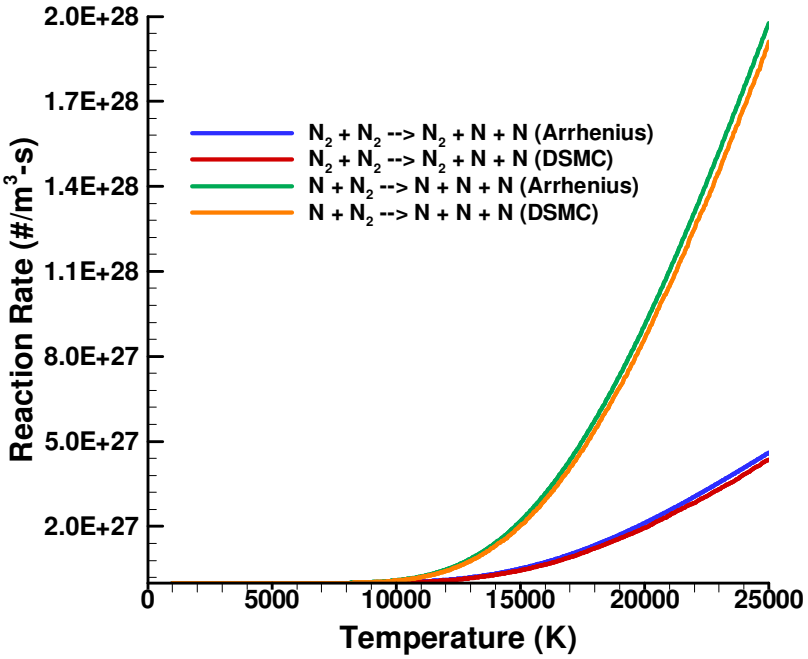

FIGURE 1. Instantaneous reaction rates for nitrogen-only reactions at various temperatures. Number densities of N_2, N, O_2, O, and NO are all set at 2.0×10^{22} #/m^3. The temperatures shown here are total temperatures, and the diatomic species are initialized with their rotational and vibrational modes in equilibrium with the translational mode.

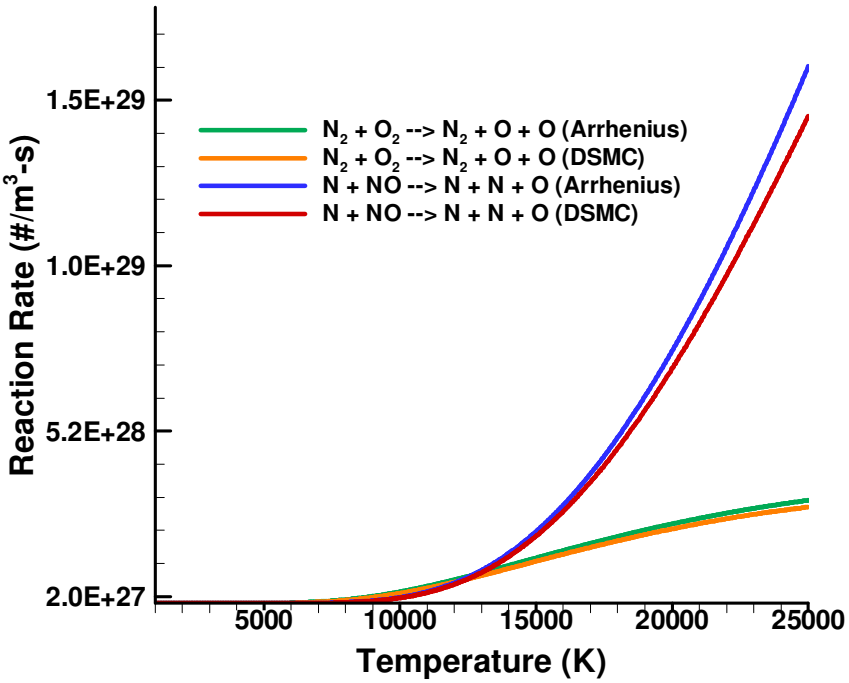

FIGURE 2**.** Instantaneous reaction rates for O_2 and NO dissociation reactions as a function of temperature. Only two sample reactions are shown, although the entire reaction set is enabled. Initial conditions are the same as in Fig. 1.

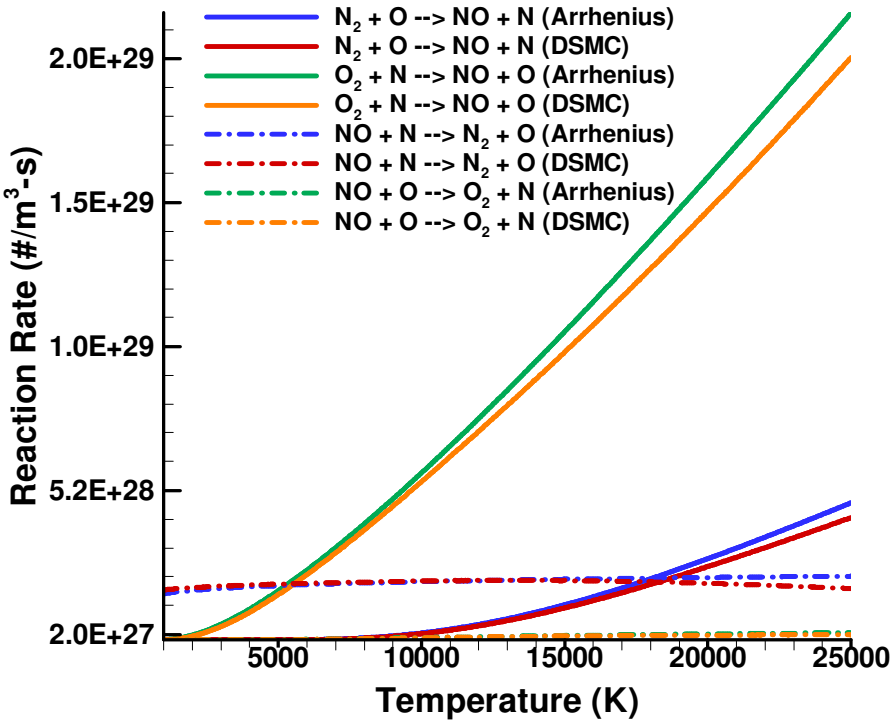

FIGURE 3**.** Instantaneous reaction rates for NO exchange reactions as a function of temperature. Initial conditions are the same as in Fig. 1.

The DSMC code is MPI parallel. For a given simulation, each processor is initially assigned a set of individual 0-D relaxations (all with the same initial conditions), and a given processor handles initialization, collisions, reactions, and any other required work for each relaxation, completing one and then moving on to the next, up to its allotted number. When all processors have completed their set of relaxations (each individual relaxation having a different random number seed), the results are ensemble averaged to obtain a smooth result. This ensemble averaging allows the inherent stochastic noise of the DSMC method to be essentially eliminated as a relevant factor, as will be shown in the following section. Note that whenever simulations are discussed later, a single simulation is understood to be composed of a number of ensemble averaged relaxations. Specifically, when we check the sensitivity of the QoI to random number seed, and we mention that 960 simulations are performed, each of these simulations is itself composed of many ensemble averaged relaxations. It is this ensemble averaging, made possible by the use of parallel processing, which allows us to render stochastic noise insignificant as a factor in the sensitivity analysis, and which will allow us to do the same in the future during the calibration process.

Sensitivity Analysis

The sensitivity analysis performed in this work serves two purposes. The primary purpose is to determine which parameters are informed by a given quantity of interest (QoI), and therefore which parameters are suitable for later calibration based on data for that QoI. The secondary purpose is to demonstrate that our results are independent of computational parameters (time step, number of simulation particles, and random number seed).

Pure Nitrogen

We must first select the set of parameters for which we will examine sensitivities, and determine the scenario to use for the analysis. Table 3 lists all the parameters examined for the pure nitrogen case, their nominal values, and the maximum and minimum values for their priors. The prior is the range of values for the parameter which would be allowed during the MCMC calibration step. Of course, while for some parameters the maximum and/or minimum are hard limits, for other parameters the range is often somewhat arbitrary. For example, in the case of Z_R (and similarly for Z_V) the lower limit of 1 is a hard limit. In the context of DSMC, a value of 1 for Z_R indicates that rotational energy is redistributed during every single collision (provided that at least one of the particles has rotational degrees of freedom). A value of $Z_R < 1$ has no meaning in this context. The nominal values of Z_R and Z_V, however, are based on values in the literature, and the upper limits are chosen to be several times larger than the nominal values, so that a reasonable range would be explored during the MCMC calibration.

Parameters #9 and #10 in Table 3 require additional explanation. They represent the pre-exponential constant in the Arrhenius rate equation (the variable A in Eq. 1) for the dissociation reactions $N_2 + N_2 \rightarrow N_2 + N + N$ and $N + N_2 \rightarrow N + N + N$, respectively. However, due to the large uncertainties in the rates, the parameter actually used here is α, where $A = 10^{\alpha}$. In this work, we treat the temperature exponent and activation energy in the Arrhenius equation (η and E_A in Eq. 1) as fixed.

Before the sensitivity analysis can be conducted, we must determine an appropriate scenario and quantity of interest (QoI). For the pure nitrogen case, the scenario is a 0-D relaxation from an initial high-temperature state. A 0-D box is initialized with 100% N_2 at a number density of 1.0×10^{23} $\#/m^3$. The initial translational temperature is ~50,000 K, and the initial rotational and vibrational temperatures are both 300 K. This is a 0-D substitute for a hypersonic shock, where we are making the assumption that the translational modes equilibrate much faster than the rotational and vibrational modes, and also before any significant chemical changes have a chance to occur. The initial translational temperature is roughly equivalent to the translational temperature which would be found directly behind a normal shock at 8000 m/s in pure nitrogen, provided the above assumption were to hold.

A simulation of this scenario was run with the nominal values for all parameters, in order to examine the results and make sure that the scenario is appropriate. The results of this run are shown in Figure 4. In the very early stages, newly dissociated nitrogen atoms are initially at a slightly lower translational temperature than the N_2 molecules. This is due to the fact that a good deal of the collision energy is absorbed during the dissociation reaction, and so until they undergo collisions with other molecules, the newly created atoms tend to have slightly lower average kinetic energy than the unreacted N_2 molecules. As more nitrogen atoms are created and undergo non-reactive collisions with N_2 molecules, the N_2 and N translational temperatures rapidly reach equilibrium. At the same time, the translational temperature of the mixture drops quickly, as the internal modes of the nitrogen molecules equilibrate with the translational mode. The nominal value for Z_R is 5, while the nominal value of Z_V is 10, so the rotational mode equilibrates first, and then the rotational temperature begins to drop as additional energy is lost to both vibration and chemical reactions. Soon after, the vibrational mode reaches equilibrium with the

rotational and translational modes, and from this point on the gas is in thermal equilibrium. The drop in temperature continues after this point, albeit more slowly, due to the energy which is lost to dissociation reactions.

Table 3: Parameters investigated during pure nitrogen sensitivity analysis.

Parameter Number	Parameter Name	Meaning	Minimum	Nominal	Maximum
1	ω (N_2-N_2)	Temperature-viscosity exponent for N_2-N_2 collisions	0.5	0.68	1.0
2	ω (N_2-N)	Temperature-viscosity exponent for N_2-N collisions	0.5	0.665	1.0
3	ω (N-N)	Temperature-viscosity exponent for N-N collisions	0.5	0.65	1.0
4	d_{ref} (N_2-N_2)	VHS reference diameter for N_2-N_2 collisions	2.00E-10 (m)	3.58E-10 (m)	5.00E-10 (m)
5	d_{ref} (N_2-N)	VHS reference diameter for N_2-N collisions	2.00E-10 (m)	3.35E-10 (m)	5.00E-10 (m)
6	d_{ref} (N-N)	VHS reference diameter for N-N collisions	2.00E-10 (m)	3.11E-10 (m)	5.00E-10 (m)
7	Z_R	Rotational collision number	1	5	10
8	Z_V	Vibrational collision number	1	10	50
9	α_1	$10^{\alpha_1} = A_1$, the pre-exponential constant in the Arrhenius rate equation for the reaction $N_2 + N_2 \rightarrow N_2 + N + N$	-8.94 (A_1 = 1.16E-9)	-7.94 (A_1 = 1.16E-8)	-6.94 (A_1 = 1.16E-7)
10	α_2	$10^{\alpha_2} = A_2$, the pre-exponential constant in the Arrhenius rate equation for the reaction $N + N_2 \rightarrow N + N + N$	-8.30 (A_2 = 4.98E-9)	-7.30 (A_2 = 4.98E-8)	-6.30 (A_2 = 4.98E-7)

Examining the densities, we see that the density of nitrogen atoms rises quickly early in the run, due to the large amount of energy available (more energy available means more collisions where $E_{collision} > E_{activation}$, and thus a reaction may take place). As the relaxation continues, the pace of reactions drops, and thus the rate of change of the densities also decreases. The densities would eventually asymptote (the beginnings of this can already be seen in Fig. 4), due to the fact that there is not enough energy available at the initial state to fully dissociation every molecule. However, this asymptotic state will not reflect the true equilibrium conditions, since we are not including recombination reactions.

We must now select a quantity of interest (QoI) for this scenario. Note that in this work, the QoI will actually be a vector which represents a given quantity at various discrete points in time. When shown in figures, these points will be displayed as part of a continuous line, but the actual QoI is a vector composed of values at discrete points.

If we were performing this work as part of a full-system validation process, we would know upfront the overall QoI. For example, the QoI for a full-system simulation of the CEV reentry might be the overall heat flux to the vehicle or the ablation rate of the thermal protection system at peak heating conditions. When performing a validation process for a sub-model, such as the radiation and thermochemistry in the shock layer, we would select a surrogate QoI which is relevant to the overall QoI. For example, for the scenario of a hypersonic shock layer, we might choose the wavelength integrated intensity of radiation at a specific point downstream of the shock as a surrogate QoI. We might also choose to integrate this intensity spatially across the post-shock region. This quantity would be related to the radiative heat flux to the vehicle in a full-system case, which in turn contributes to the overall heat flux and thus affects the ablation rate. The purpose of sensitivity analysis in this context is to determine

which parameters affect the surrogate QoI, and thus which parameters can be expected to ultimately affect the overall QoI. If the surrogate QoI is not sensitive to a particular parameter, than there is no reason to calibrate that parameter in the future, because its value does not significantly affect the model's ability to accurately predict the overall QoI.

In our case, the purpose of the sensitivity analysis is somewhat different. We are not performing this work as part of a full-system validation process, at least not initially. We are attempting to provide improved calibrations for parameters which are relevant to DSMC in general, and also to provide a framework for obtaining those improved calibrations. In this case, we have two constraints on our QoI. First, if possible our QoI should be measurable by experiment. At the very least, our QoI should be intimately related to some quantity which is experimentally observable. This is required so that the QoI can be used for future parameter calibrations. The second requirement for our QoI is that calibrations based on it must inform the parameters we wish to calibrate, thus we must choose a QoI which is sensitive to those parameters. Of course, we may not be able to find a QoI which is sensitive to all parameter we wish to calibrate, and which is also related directly to experimental data, and in that case we will need to pick the one that informs as many of the parameters we most wish to calibrate as possible. Thus, the purpose for our sensitivity analysis is different from the purpose of a sensitivity analysis in the context of a full-system validation process. We will use sensitivity analysis to determine both which parameters we will be able to calibrate, and also which QoI (out of those which might reasonably be available from experiment) will allow us to do the best calibration possible for as many of our parameters as possible.

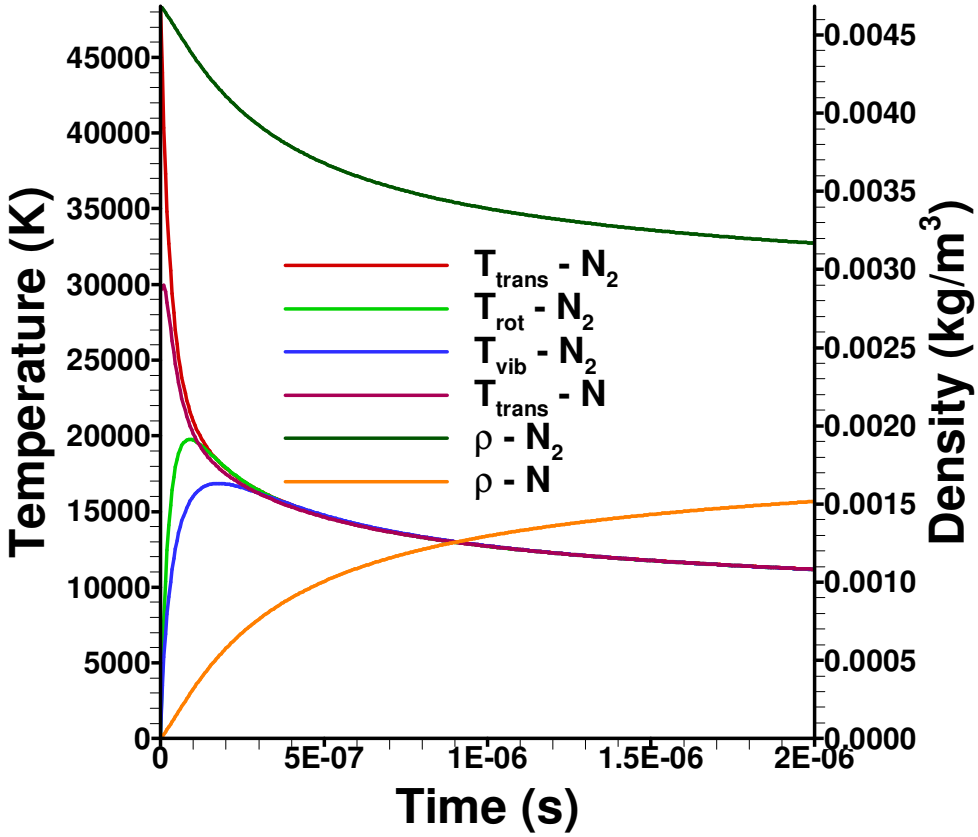

FIGURE 4. Mass densities and temperatures of N_2 and N as functions of time for a 0-D relaxation with the nominal values of all parameters. Initial composition is 100% N_2, with number density of 1.0×10^{23} #/m^3. Initial translational temperature is 50000 K, and initial rotational and vibrational temperatures are both 300 K.

For the pure nitrogen sensitivity analysis in this work, we have chosen the translational temperature of the atomic nitrogen as the QoI. We are doing the pure nitrogen case as an example of our sensitivity analysis methodology, so for this case only one QoI was chosen. We will use two different QoIs for the five-species air sensitivity analysis, and in the future we will examine others. For the present, $T_{trans,N}$ was chosen as the QoI because, according to Johnston (2008), a significant portion of the radiation which is measured in the EAST shock tube

comes from atomic line transitions of nitrogen and oxygen. The intensity of these atomic lines can be related, with some assumptions, to the temperature of those species. Therefore, with our current code, $T_{trans,N}$ provides a QoI which is directly related to an experimental observable which we could potentially make use of in future calibrations. The QoI vector for the case with all parameters at their nominal values is shown in Figure 5.

The methods used here for sensitivity analysis are fairly simple. We examine the sensitivity of the QoI to each parameter in turn (we do not consider coupling between the parameters in this work). The procedure for checking sensitivity is as follows:

1.) Run a simulation and obtain results for the QoI with a value for parameter 1 which is greater than the nominal value, and with the nominal values for all other parameters. How this higher value of parameter 1 is chosen will be discussed shortly.

2.) Run a simulation with a value for parameter 1 which is less than the nominal value, and with the nominal values for all other parameters.

3.) Calculate the vector $\mathbf{\Delta QoI_{param1} = QoI_{param1,high} - QoI_{param1,low}}$, as shown in Figure 6.

4.) Repeat steps 1-3 for each parameter.

5.) Compare the $\mathbf{\Delta QoI}$ vectors for each parameter in order to rank parameters based on sensitivity. We use the value $(\mathbf{\Delta QoI})^T(\mathbf{\Delta QoI})$ to provide a single number which represents the sensitivity to a given parameter.

The key step in the above procedure is determining what to use for the high and low values of each parameter. We have employed three methods for this, and results from all three will be shown for the pure nitrogen case. In the first method, we use the full range of the parameter which would be used as the prior during future calibration of that parameter (i.e. we use the maximum and minimum values shown in Table 3). The advantage of this method is that it accounts for variation in the QoI with respect to the parameters over a broad range of each parameter. The disadvantage is that the final value calculated for the sensitivity to each parameter is highly dependent on the range chosen for the parameter.

A second method for choosing the high and low values is to use a percentage of the total range of the parameter. For example, if the percentage to be used was 10%, then

$$\mathrm{Param1}_{high} = \mathrm{Param1}_{nominal} + (\mathrm{Param1}_{maximum} - \mathrm{Param1}_{nominal})\times 0.1,$$

and similarly,

$$\mathrm{Param1}_{low} = \mathrm{Param1}_{nominal} - (\mathrm{Param1}_{nominal} - \mathrm{Param1}_{mininum})\times 0.1.$$

This method focuses on the sensitivity in the region of the nominal value, but still takes account for size of the overall range of the parameter. The first method is really a special case of this method, of course, where the percentage used is 100%.

The third method does not make use of the range of the parameter, but only the nominal value. In this case, the high and low values of each parameter are based on adding or subtracting a percentage of the nominal value. Using 10%, for example,

$$\mathrm{Param1}_{high} = \mathrm{Param1}_{nominal} + \mathrm{Param1}_{nominal}\times 0.1$$

and

$$\mathrm{Param1}_{low} = \mathrm{Param1}_{nominal} - \mathrm{Param1}_{nominal}\times 0.1.$$

The advantage of this method is that it does not require information on the range of the parameter, and therefore may be somewhat less arbitrary, at least for a parameter where the nominal value is fairly well known. Of course, this advantage can also be a disadvantage, since the plausible range of some parameters is larger than that of others, and therefore it is necessary to account for sensitivity of the QoI to those parameters in regions away from the nominal value.

We used all three methods described above for the pure nitrogen sensitivity analysis, both to make the best possible decision concerning which parameters to calibrate in the future, and also to evaluate the utility of the three methods. In addition to the physical parameters shown in Table 3, we also tested the sensitivity of the QoI with respect to the time step, the ratio of real to simulated particles, and the random number seed. In order to test the sensitivity to time step, we ran a case with the nominal values of all other parameters, but with a time step which was half as long as that used for the rest of the simulations, and another case with a time step twice as long as the one normally used. Similarly, runs were done with half and also with twice the normal ratio of real to simulated particles. We then calculated the $\mathbf{\Delta QoI}$ vector and $(\mathbf{\Delta QoI})^T(\mathbf{\Delta QoI})$ for time step and for real to simulated particle ratio as we did for the other parameters. Even when doing the second or third methods for sensitivity analysis, we still halved and doubled the time step and ratio of real to simulated particles, rather than doing a percentage change as for the other parameters. So, when we show later that the sensitivities for the time step and ratio of real to simulated particles are very low compared to that for other parameters, even for methods two or three, we are showing that the QoI is much more sensitive to a 10% change in the other parameters than it is to a factor of four

difference in the time step or ratio of real to simulated particles. We did it this way because we wanted to be very conservative in making sure that our results were not affected by computational parameters.

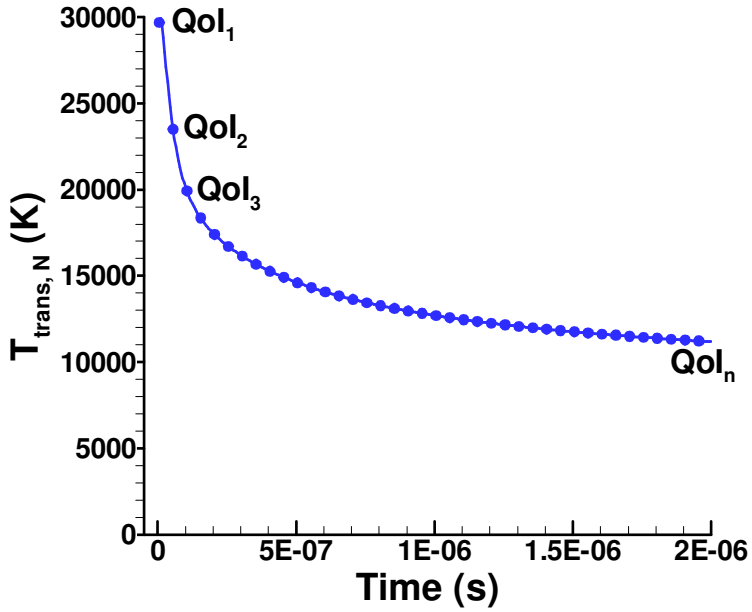

FIGURE 5. Schematic showing the definition of the QoI for the pure-nitrogen sensitivity analysis.

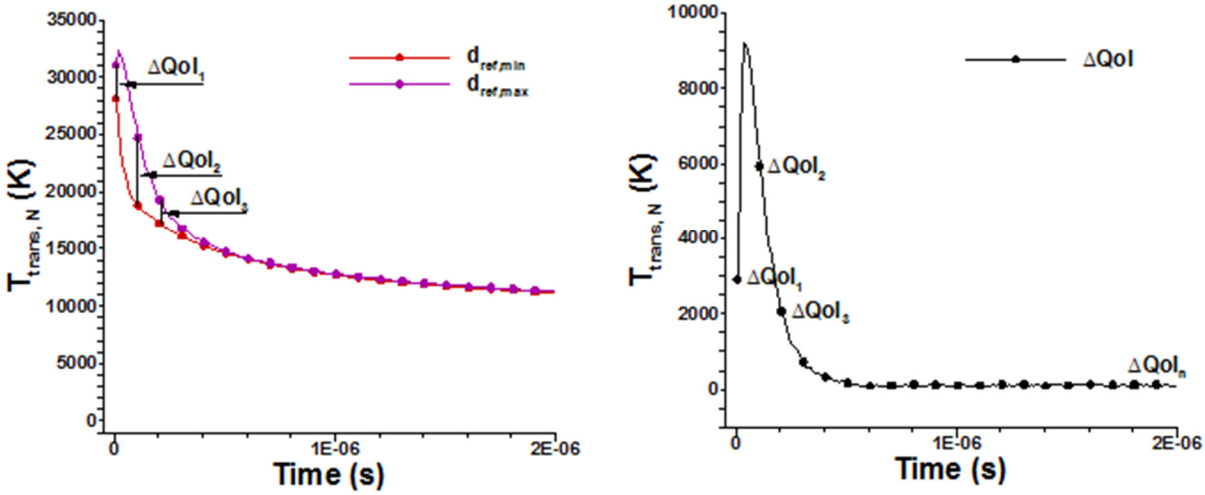

FIGURE 6. Schematic showing the definition of ΔQoI for the pure nitrogen sensitivity analysis.

In order to test sensitivity to random number seed (i.e. sensitivity to the stochastic noise inherent in DSMC), a total of 960 simulations were performed, and at each output point (QoI_1, QoI_2, etc., as shown in Fig. 5), the maximum and minimum values out of all the 960 simulations were found. The value of the **ΔQoI** vector at each point is then the difference between the maximum value (out of all 960 simulations) at that point and the minimum value (again out of all 960 simulations) at that point. We can then calculate $(\mathbf{\Delta QoI})^T(\mathbf{\Delta QoI})$ as for the other parameters. This means that, when we show later that the QoI is significantly more sensitive to most of the parameters than to random number seed, we are showing that a 10% change in a parameter value leads to a significantly larger change in the QoI than the change in the QoI which results from the stochastic noise inherent in DSMC.

The results obtained with all three sensitivity analysis methods are shown in Table 4 and Figure 7. Parameters #1-10 in Fig. 7 are those numbered in Table 3. Parameters 11, 12, and 13 correspond to the time step, ratio of real to simulated particles, and random number seed, respectively. The sensitivity value shown for each parameter is a normalized sensitivity, given by

$$Normalized\ Sensitivity\ = \frac{(\mathbf{\Delta QoI})^T(\mathbf{\Delta QoI})}{(\mathbf{\Delta QoI})^T(\mathbf{\Delta QoI})_{max}}$$

where $(\mathbf{\Delta QoI})^T(\mathbf{\Delta QoI})_{max}$ is the maximum sensitivity value for any parameter. The top row shows sensitivities based on the first method, the middle row is for the second method, and the bottom row is for the third method. It is clear from Fig. 7 that the QoI is much more sensitive to some parameters than to others. The vertical axis of the chart on the right in each row is saturated, so that the sensitivities to parameters other than the two reaction rates can be examined. Figure 7 also makes clear that the QoI is far more sensitive to many of the parameters than it is to the computational parameters or to the stochastic noise.

In Table 4, the parameters are ranked by sensitivity for each method. The top two parameters are the same for all three methods, and the parameters in the top eight are also the same for all three methods, although the order does change. The parameters are not ranked below 8, because the 9th ranked "parameter" would be the stochastic noise, and ranking parameters below this level would be pointless. Note, however, that there are only two physical parameters which go unranked: the reference diameter and temperature viscosity exponent for N-N collisions. That is, the QoI is quite insensitive to those two parameters. The time step and real to simulation particle ratios are also ranked below the stochastic noise. When doing the calibration, we would calibrate only the top six parameters, because while parameters 7 and 8 are ranked higher than the stochastic noise, they are still relatively close to that limit. In all three methods, the sixth most sensitive parameter has a normalized sensitivity which is several times higher than the normalized sensitivity value for the stochastic noise.

We can get more information about these sensitivities by plotting the vector of absolute values of **ΔQoI** for the six parameters to which the QoI is most sensitive, as is done in Figure 8. The **ΔQoI** vector for the random number seed sensitivity check is also shown in the figure. Figure 8 is based on the second sensitivity method, but the trends are similar for the other two methods as well. Figure 8 explains why the sensitivities to the reaction rates are so much higher than the others. While the QoI is very sensitive to the N_2-N_2 VHS parameters and Z_R and Z_V in the early part of the simulation, it is almost completely insensitive to them once the gas mixture has reached thermal equilibrium. The QoI remains sensitive to the reaction rates throughout the simulation, however. It can also be seen from the figure that even in the early stages, when there are relatively few nitrogen atoms, the QoI is still significantly more sensitive to the sixth ranked parameter (Z_R) than it is to stochastic noise.

Table 4: Sensitivity analysis results for pure nitrogen.

Sensitivity Rank	Sensitivity Type 1	Sensitivity Type 2	Sensitivity Type 3
1	α_2	α_2	α_2
2	α_1	α_1	α_1
3	ω (N_2-N_2)	Z_V	ω (N_2-N_2)
4	d_{ref} (N_2-N_2)	ω (N_2-N_2)	d_{ref} (N_2-N_2)
5	Z_V	d_{ref} (N_2-N_2)	Z_R
6	Z_R	Z_R	Z_V
7	d_{ref} (N_2-N)	d_{ref} (N_2-N)	ω (N_2-N)
8	ω (N_2-N)	ω (N_2-N)	d_{ref} (N_2-N)

Five-Species Air

A second sensitivity analysis was conducted for a 0-D relaxation of five-species air, with the reaction set listed in Table 2. The initial conditions were very similar to that used for the pure nitrogen analysis, except this time rather than 100% N_2, the initial composition was 79% N_2 and 21% O_2, by volume. For both species the initial translational temperature was ~50000 K, and the initial rotational and vibrational temperatures were 300 K. Only dissociation and exchange reactions were modeled, recombination was not included.

Figure 9 shows the evolution of the species mass densities. The N_2 and O_2 densities drops rapidly as both dissociation and exchange reactions take their toll. O_2 is soon fully dissociated, but the N_2 density levels off as the temperature drops and the reactions slow. The densities of atomic oxygen and nitrogen rise rapidly, and then level off. The most interesting is the density of NO, which initially rises rapidly due to exchange reactions which are

dominant at high temperatures, but then levels off and eventually drops as the overall temperature drops and dissociation becomes dominant and NO molecules are split apart more quickly than they are formed via exchange reactions.

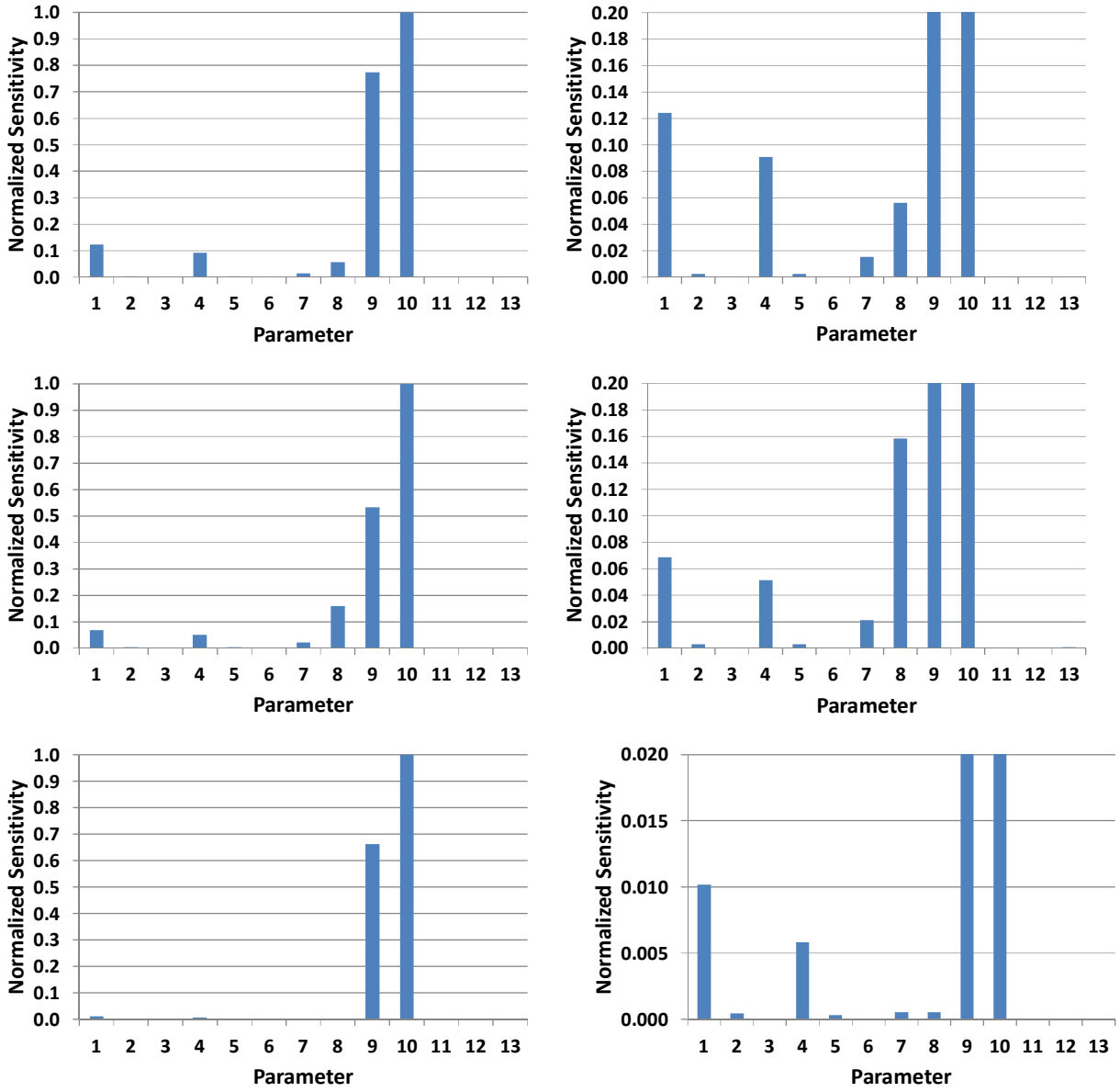

FIGURE 7. Results for the three types of sensitivity analysis for the pure nitrogen case. Parameter #'s 1-10 correspond to parameter #'s 1-10 in Table 3. Parameters 11-13 represent the ratio of real to simulated particles, the time step, and the random number seed, respectively. Top row is for type 1 sensitivity analysis, middle row is for type 2, and bottom row is for type three. The right image in each row saturates the normalized sensitivity, so that moderately sensitive parameters may be examined.

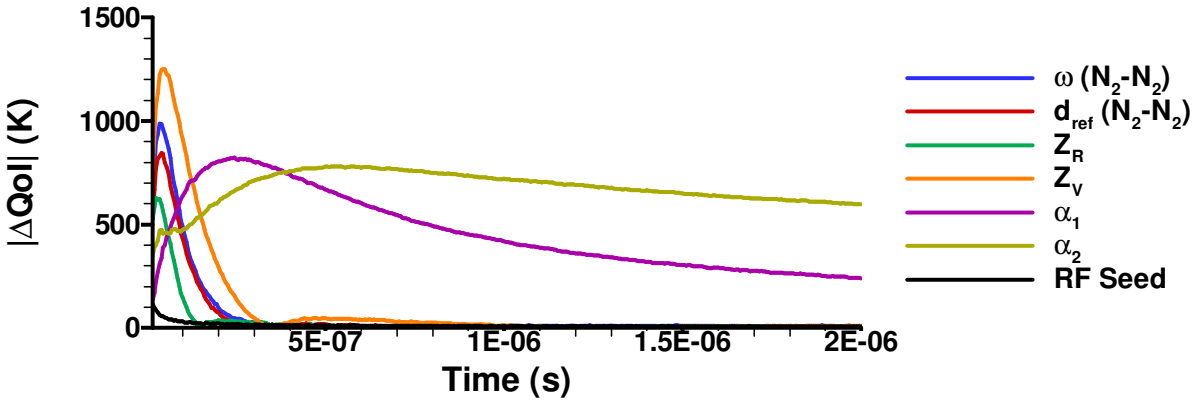

FIGURE 8. |ΔQoI| as a function of time for the top six most sensitive parameters for the pure nitrogen case, as well as for the random number sensitivity analysis.

Figure 10 focuses on the translational temperatures near the beginning of the simulation. As in the pure nitrogen case, the translational temperatures of the atomic species are lower during the very early part of the simulation. In each collision that leads to a dissociation reaction, a portion of the collision energy is "lost" to chemical potential energy. In many cases, this lost energy is a significant fraction of the total collision energy, and therefore the average post-collision kinetic energy for the newly dissociated atomic species is lower than the average kinetic energy of the molecular species which have not undergone chemical reactions, and therefore have not lost energy. Very soon, however, the translational modes of the various species equilibrate due to elastic collisions. Note that the NO molecules which exist at this stage are formed via exchange reactions, one of which is endoergic but with a lower amount of energy absorbed than the dissociation reactions, and the other of which is actually exoergic, and therefore the difference in translational temperature between NO and the O_2 and N_2 is relatively small even at the earliest stages.

Figure 11 shows the translational temperatures of the various species over the entire course of the simulation. As in the pure nitrogen case, the translational temperatures drop rapidly as the internal modes equilibrate with the translational mode and simultaneously energy is lost to chemical reactions. After thermal equilibrium is reached , the translational temperatures drops more slowly because no more net energy is being shifted from translational to internal modes. Also, as the temperature drops, the reaction rates drop, and this leads to a lower rate of change of the temperature, since after thermal equilibrium is reached it is chemical reactions which drive the temperature change.

With the scenario defined, two sensitivity analyses were performed for the 5-species air case, each with a different QoI. The first analysis was performed with the same QoI as in the pure nitrogen case, namely the translational temperature of atomic nitrogen. The second analysis was performed using the mass density of NO as the QoI.

Since the sensitivities to reaction rates dominated all others in the pure nitrogen case, only the reaction rates were used as parameters for the 5-species case. As before, the parameter examined for each reaction is α, where the pre-exponential constant in the Arrhenius rate equation, A, is equal to 10^{α}. Once again, we treat the temperature exponent and activation energy in the Arrhenius equation (η and E_A in Eq. 1) as fixed. We would like to vary the pre-exponential constant by a total of two orders of magnitude (allowing it to be up to one order of magnitude smaller or one order of magnitude larger), and therefore the full range of α for each reaction is from α_{nom}-1 to α_{nom} + 1 (i.e. for each reaction, $\alpha_{min} = \alpha_{nom} - 1$, and $\alpha_{max} = \alpha_{nom} + 1$).

Based on the results of the pure nitrogen analysis, both analyses performed here used the second method described above (with 5% as the percentage of the range, as in the pure nitrogen case). Therefore, for each reaction, the low value of $\alpha = \alpha_{nom} - 0.05$, and the high value of $\alpha = \alpha_{nom} + 0.05$. Sensitivities to time step, ratio of real to simulated particles, and stochastic noise were also determined in the same method as before.

Results for the 5-species air sensitivity analyses are shown in Table 5 and Figures 12 and 13. It is clear from Fig. 12 and 13 that the same two reaction rates (really the forward and backward rates for one exchange reaction, $N_2 + O \leftrightarrow NO + N$) have the dominant sensitivities for either QoI. Furthermore, when examining only the sensitivities of the rates for the NO dissociation reactions and the NO exchange reactions relative to one another (i.e. looking only at the right half of Figs. 12 and 13), the two analyses are quite similar. However, the first QoI, $T_{trans,N}$, is also sensitive to several of the nitrogen dissociation reactions and one of the oxygen dissociation reactions (O_2 +

$O_2 \rightarrow O_2 + O + O$), while the second QoI, ρ_{NO}, is almost totally insensitive to these rates, at least in comparison to its sensitivity to various NO related reactions. This is somewhat surprising, since in order for NO to form at all there must be dissociated nitrogen and/or oxygen present (we do not include the reaction $N_2 + O_2 \rightarrow 2NO$ since it is presumably very rare). This is perhaps an example of a case where it would have been useful to examine sensitivities at the edges of the range of each parameter, and not only about the nominal.

The various reaction rates are ranked based on sensitivity for each QoI in Table 5. In the case of $T_{trans,N}$ as the QoI, the stochastic noise would be the 16th most sensitive parameter, and in the case of ρ_{NO} as the QoI, it would be the 19th most sensitive. Both QoIs are less sensitive to the time step and ratio of real to simulated particles than to stochastic noise. For the $T_{trans,N}$ as QoI case, there are four reactions which are unranked, due to the fact that the QoI is less sensitive to them than to stochastic noise. Those reactions are #'s 10, 13, 15, and 19 in Table 2. The only unranked reaction in the case with ρ_{NO} as QoI is #10.

It would most likely be possible to calibrate the top eight or even top eleven ranked reactions when using $T_{trans,N}$ as QoI, but it would probably be best to calibrate only the top six ranked reactions (all of which are NO related) when using ρ_{NO} as QoI.

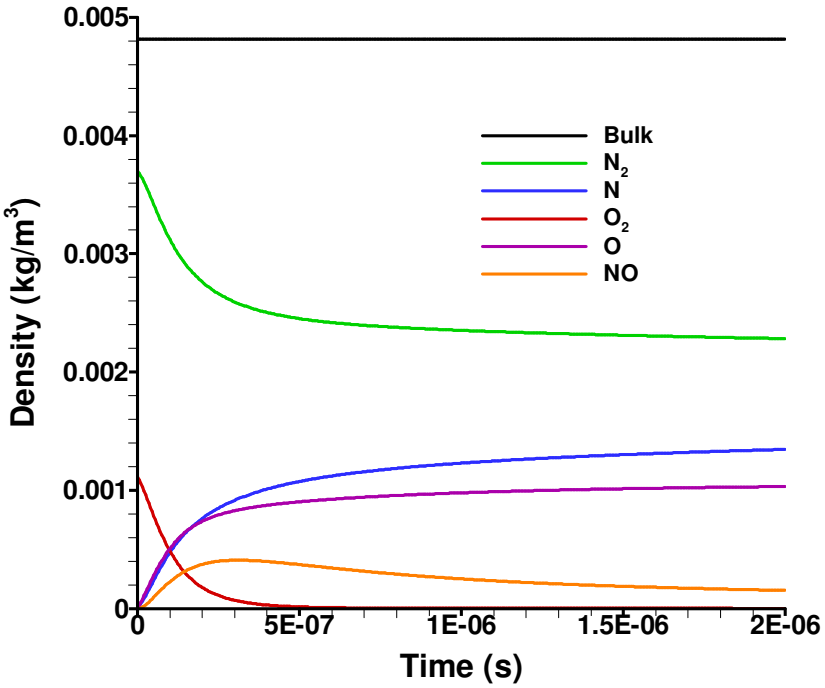

FIGURE 9. Mass densities of the 5 species as functions of time for a 0-D relaxation with the nominal values of all parameters. Initial concentrations are 79% N_2 and 21% O_2 (by volume), with total number density of 1.0×10^{23} #/m^3. Initial translational temperature is 50000 K, and initial rotational and vibrational temperatures are both 300 K.

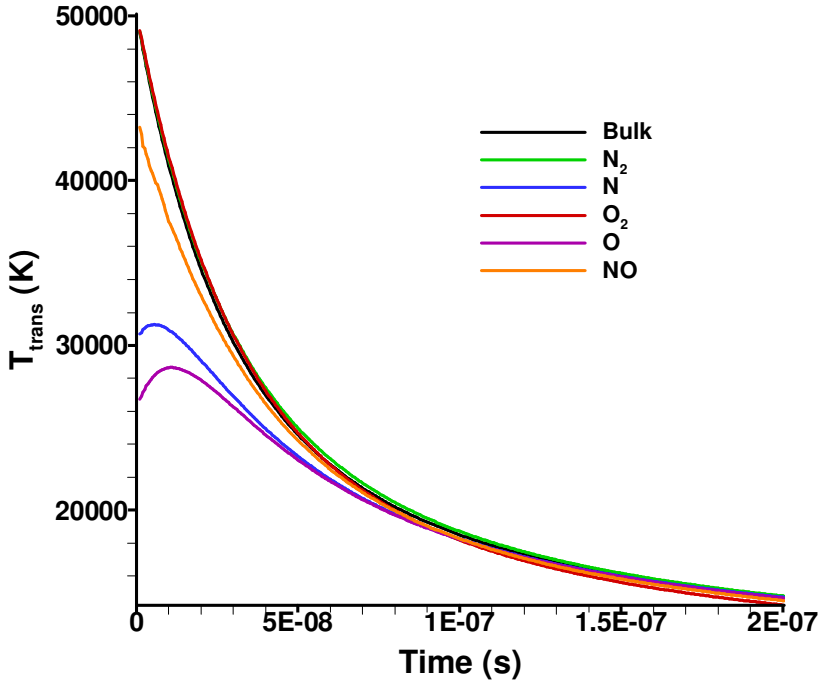

FIGURE 10**.** Translational temperatures of the 5 species as functions of time for a 0-D relaxation with the nominal values of all parameters, showing the earliest part of the simulation.

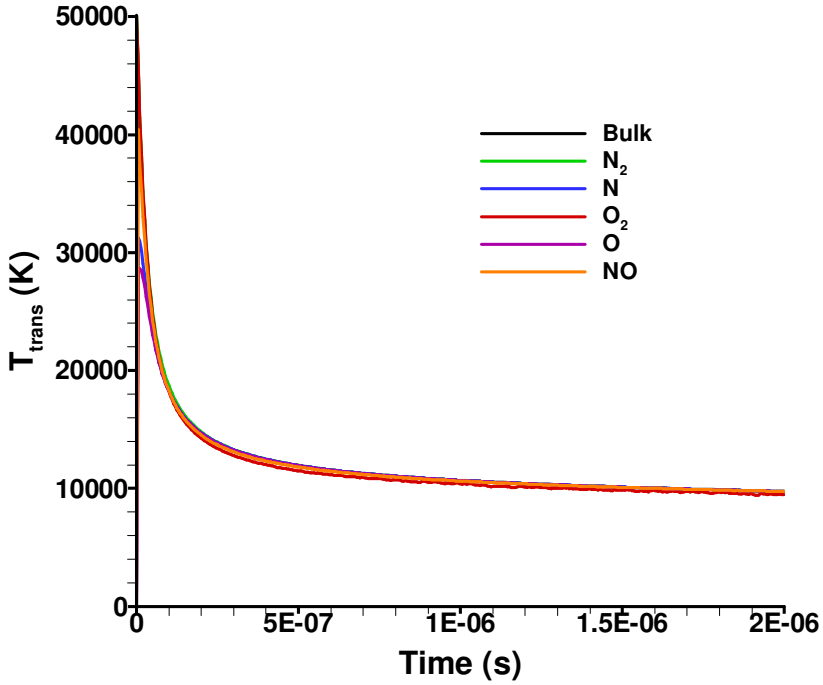

FIGURE 11**.** Same data as Fig. 10, now showing the full simulation. Initial conditions are the same as for Fig. 9.

Table 5: Sensitivity analysis results for 5-species air.

Sensitivity Rank	QoI = $T_{trans,N}$		QoI = ρ_{NO}	
	Equation	Reaction #	Equation	Reaction #
1	$N_2 + O \rightarrow NO + N$	16	$N_2 + O \rightarrow NO + N$	16
2	$NO + N \rightarrow N_2 + O$	18	$NO + N \rightarrow N_2 + O$	18
3	$N + N_2 \rightarrow N + N + N$	2	$N_2 + NO \rightarrow N_2 + N + O$	11
4	$N_2 + NO \rightarrow N_2 + N + O$	11	$O_2 + N \rightarrow NO + O$	17
5	$N_2 + N_2 \rightarrow N_2 + N + N$	1	$N + NO \rightarrow N + N + O$	12
6	$O + N_2 \rightarrow O + N + N$	4	$O + NO \rightarrow O + N + O$	14
7	$N_2 + O_2 \rightarrow N_2 + O + O$	6	$N + N_2 \rightarrow N + N + N$	2
8	$N + NO \rightarrow N + N + O$	12	$N_2 + O_2 \rightarrow N_2 + O + O$	6
9	$O_2 + N \rightarrow NO + O$	17	$O + N_2 \rightarrow O + N + N$	4
10	$O + NO \rightarrow O + N + O$	14	$N_2 + N_2 \rightarrow N_2 + N + N$	1
11	$O_2 + N_2 \rightarrow O_2 + N + N$	3	$O_2 + N_2 \rightarrow O_2 + N + N$	3
12	$N + O_2 \rightarrow N + O + O$	7	$N + O_2 \rightarrow N + O + O$	7
13	$O_2 + O_2 \rightarrow O_2 + O + O$	8	$NO + NO \rightarrow NO + N + O$	15
14	$O + O_2 \rightarrow O + O + O$	9	$O + O_2 \rightarrow O + O + O$	9
15	$NO + N_2 \rightarrow NO + N + N$	5	$NO + N_2 \rightarrow NO + N + N$	5
16	-	-	$NO + O \rightarrow O_2 + N$	19
17	-	-	$O_2 + O_2 \rightarrow O_2 + O + O$	8
18	-	-	$O_2 + NO \rightarrow O_2 + N + O$	13

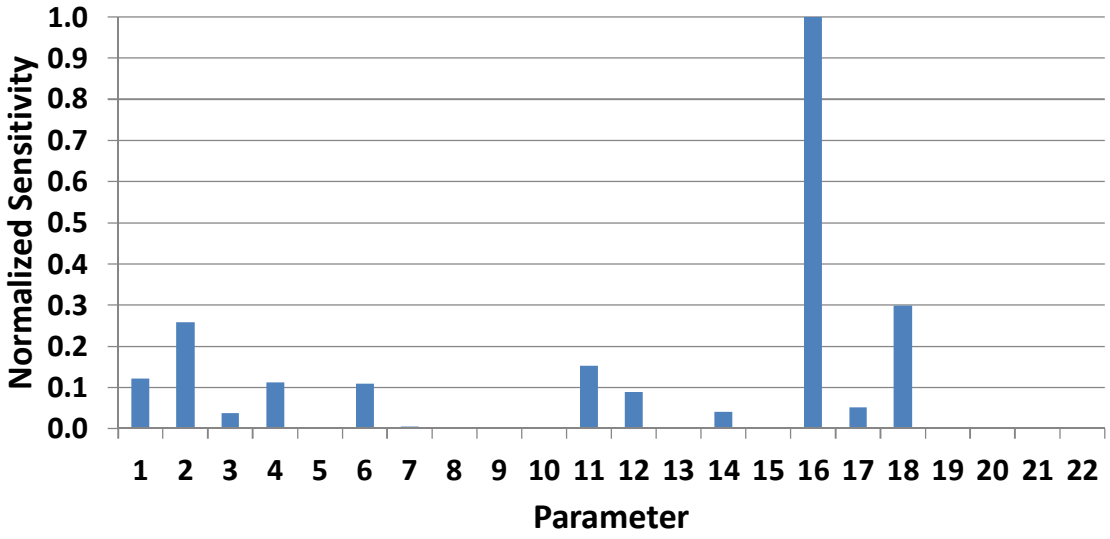

FIGURE 12**.** Results for 5-species sensitivity analysis using $T_{trans,N}$ as the QoI. Parameter #'s 1-19 correspond to reaction #'s 1-19 in Table 2. Parameters 20-22 represent the ratio of real to simulated particles, the time step, and the random number seed, respectively.

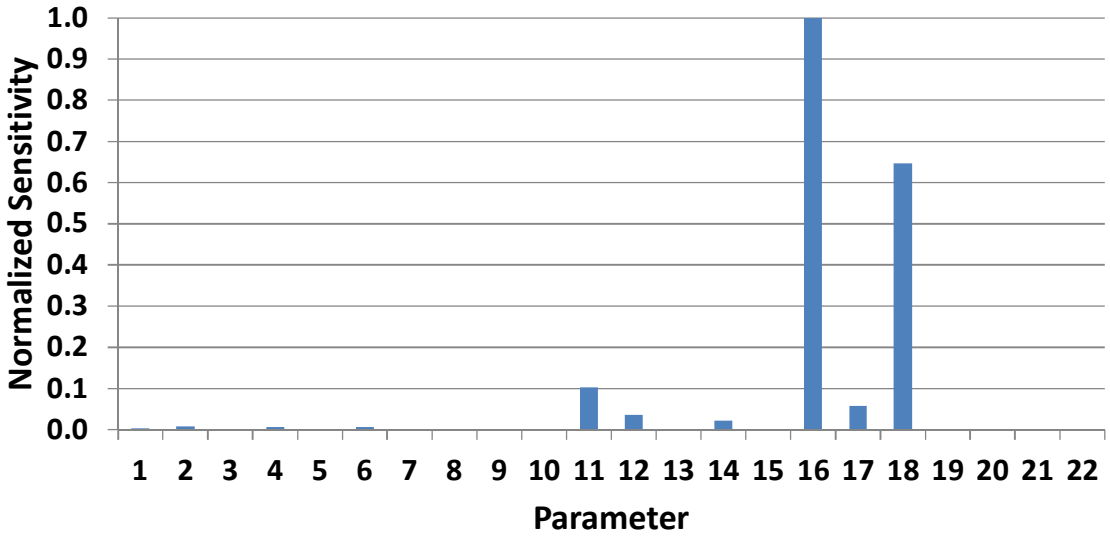

FIGURE 13**.** Results for 5-species sensitivity analysis using ρ_{NO} as the QoI. Parameter #'s 1-19 correspond to reaction #'s 1-19 in Table 2. Parameters 20-22 represent the ratio of real to simulated particles, the time step, and the random number seed, respectively.

Conclusions

The primary purpose of this work was to develop a set of methods for sensitivity analysis which can be employed to rank DSMC parameters based on sensitivity for a given QoI, and thus to properly choose parameters for calibration which will be informed by the available data. We have also discussed a 0-D relaxation case which can be used as a proxy for a hypersonic shock, at least in some respects.

Sensitivity analyses based on this 0-D relaxation scenario allowed us to rank parameters for a pure nitrogen case and determine that sensitivities for the reaction rates dominate those for the other DSMC parameters. We have also used our sensitivity analysis methodology to demonstrate that our results are independent of time step and the ratio of real to simulated particles, and that stochastic noise can be removed as a factor if sufficient ensemble averaging is used.

For the five-species air case, we have shown that the sensitivities for the forward and backward rates for the reaction $N_2 + O \leftrightarrow NO + N$ are dominant when using either $T_{trans,N}$ or ρ_{NO} as the QoI. Some other NO related reactions have moderate sensitivities with either QoI. Several of the nitrogen dissociation reactions and the oxygen dissociation reaction $O_2 \rightarrow O_2 + O + O$ also have moderate sensitivities when using $T_{trans,N}$ as the QoI, but these reactions have insignificant sensitivities when using ρ_{NO} as the QoI.

The next step for us is to perform calibrations with synthetic data, in order to demonstrate that the statistical inverse problem is solvable before moving on to real data.

Acknowledgements

Computing resources and funding for this project were provided by the DOE though the PSAAP program. Several members of the PECOS research staff provided valuable knowledge and advice which aided our work.

References

H. Alsmeyer, "Density Profiles in Argon and Nitrogen Shock Waves Measured by the Absorption of an Electron Beam", *Journal of Fluid Mechanics* (1976), Vol. 74, Part 3, pp. 497-513.

G. A. Bird, *Molecular Gas Dynamics and the Direct Simulation of Gas Flows*, Oxford Univ. Press. Oxford, 1994.

C. Borgnakke and P. S. Larsen, "Statistical collision model for Monte Carlo simulation of polyatomic gas mixture", *Journal of Computational Physics* (1975), Vol. 18, Issue 4, pp. 402-420.

J. Grinstead, M. Wilder, and J. Olejniczak, D. Bogdanoff, G. Allen, and K. Danf, "Shock-Heated Air Radiation Measurements at Lunar Return Conditions", AIAA Paper 2008-1244, 2008.

C. O. Johnston, "A Comparison of EAST Shock-Tube Radiation Measurements with a New Radiation Model", AIAA Paper 2008-1245, 2008.

T. Ozawa, J. Zhong, and D. A. Levin, “Development of kinetic-based energy exchange models for noncontinuum, ionized hypersonic flows”, *Physics of Fluids* (2008), Vol. 20, Paper #046102.